Int. J. Electrochem. Sci., 12 **(2017)** 11030 – 11041, doi: 10.20964/2017.11.101

International Journal of
ELECTROCHEMICAL
SCIENCE
www.electrochemsci.org

Development of a Highly Efficient 3D RuPdBi/NG Electrocatalyst for Ethylene Glycol Oxidation in an Alkaline Media

Yaxi Pan, Menghuan Chen, Si Wu, Yue Li, Di Lu, Hongkun Xu, Weiwei Peng and Liqun Zhou[*]

Hubei Collaborative Innovation Center for Advanced Organic Chemical Materials, Ministry of Education Key Laboratory for the Synthesis and Application of Organic Functional Molecules, College of Chemistry and Chemical Engineering, Hubei University, Wuhan 430062, People's Republic of China.
[*]E-mail: zhoulq2003@163.com & 15872361774@163.com

Received: 14 June 2017 / *Accepted:* 25 July 2017 / *Published:* 12 October 2017

Palladium (Pd) based catalysts are being considered as one of the most attractive area of research among researchers in recent years. These catalysts are used in the alcohol oxidation in fuel cells, despite it results in not enough higher oxidation efficiency. Following this to improve the efficiency changes in the structure of the catalyst and improving the loaded metal seem to be a reasonable approach. In this investigation, design and synthesis of a three-dimensional nitrogen-doped graphene (3D-NG)-loaded with palladium, ruthenium and bismuth have been proposed. The resultant three-dimensional structure provides a larger surface area, meanwhile, the synergistic effect of RuPdBi/NG tri-metal catalyst promotes the electro-oxidation rate of ethylene glycol. The catalytic activity of palladium layer in the catalyst was enhanced owing to the surface modification and electronic effect. The cyclic voltammetry and chronoamperometry techniques showed that 3D RuPdBi/NG has a higher catalytic activity and durability than the commercial Pd/C, 3D Pd/NG and 3D RuPd/NG.

Keywords: SiO_2 temple; Nitrogen-doped graphene; tri-metallic catalyst; ethylene glycol electro-oxidation; application possibility.

1. INTRODUCTION

In the recent decades, investigations are directed toward one of the most promising energy conversion technologies of direct alcohol fuel cell (DAFC) for the oxidation of smaller organic molecules. Due to their high energy conversion efficiency, environment friendly nature and easy to use

[1], DAFC are mainly based on platinum polymetallic anode catalysts in an acidic media. But these Pt-based catalysts still do not meet the requirements of commercialization due to their low catalytic performance, poor storage, and high price [2-4]. a new anode is needed [5]. The Pd-loaded catalysts are being applied to DAFC which has come to our field of vision. The Pd-loaded anode catalyst is a highly attractive candidate as it has higher electrocatalytic activity and resistance to poisoning compared to Pt in an alkaline medium [6-19]. In addition, Pd is cheaper and has more storage on earth than Pt [20]. Moreover, the palladium-based catalyst has made great progress in catalysis mainly due to its stability making it practically feasible for a diverse technological applications.

In recent studies, intense efforts have been devoted to improving the activity of Pd catalysts, by introducing some metallic and nonmetallic elements such as Cu, B, P and Bi to graphene to optimize the catalytic performance [3,21,22]. For instance, it was reported the ways of sputtering Au and Pd into room temperature ionic liquids to promote catalytic properties of the thermometal mechanism [23]. RuPd doped Bi core-shell catalyst was also used to enhance the electro-oxidation ability of ethylene glycol via the core-shell mechanism of modification [24]. Furthermore, besides graphene, a range of carbon materials such as nanotubes and nanofibers are the most commonly used catalytic materials. However, they are less conductive and less durable than graphene [25]. The limiting case is that high graphite materials always have low surface area [26-30]. It has been reported that SiO2-modified graphene could increase the surface area [31]. It is an effective way to improve the catalytic performance by promoting the loaded metal activity and changing the structure. However, the understanding of the synergistic effect of metallization and structural transformation is still very limited. To the best of our knowledge, there are only a few investigations reported on the study of feasibility of a three-metal or multi-metal nanoparticles with a synergistic effect to improve the activity of the catalyst. In this work, a new 3D RuPdBi nitrogen-doped graphene (NG) nano-catalyst has been synthesized based on a deposition technique via two-steps. Due to the high energy density, low toxicity and ethylene glycol permeability of the membrane, the catalytic performance of RuPdBi/NG catalyst on ethylene glycol was studied in detail. Moreover, the catalytic performance of Pd/C, 3D Pd/NG and 3D RuPd/NG have been compared.

2. EXPERIMENTAL SECTION

2.1 Sample preparation

The RuPdBi/NG catalyst was synthesized via the following steps: (i) the modified Hummers method was used to synthesise graphite oxide [32, 33], (ii) the preparation of N-doped graphene: Graphene oxide (GO) (40 mg) was ultrasonicated in deionized water (30 mL), then urea (1.2 g) was added to the above dispersion and was stirred vigorously for 30 min. and then placed in a sealed Teflon-lined autoclave (50 ml). This was then kept in an oven at 165 ℃ for 3h. Following this, the Teflon-lined autoclave was cooled to room temperature, and the mixture was filtered through a type if filter membrane and washed several times with absolute ethyl alcohol and then distilled water. Finally, the obtained products were dried in vacuum oven at 80 ℃ for overnight [34]. (iii) the preparation of 3D N-doped graphene: 20 mg of nano silica template (99.5%, 50±5nm) was infused into the mixture of

water and 10 mg of exfoliated GO (SiO_2: GO in 2:1 by weight), then was subjected to stirring for 2h, and then dried at 60 ℃in a vacuum oven for overnight [34, 35].

In order to synthesize specific 3D RuPdBi/NG (2:1:0.1), 20 mg 3D NG and 18 mL of 10.0 mM $RuCl_3$ were dispersed in 50 mL ethylene glycol under ultrasonic stirring for 1 h. Then 95 mg of $NaBH_4$ was dissolved into 50 mL deionized water. $NaBH_4$ solution was then added dropwise to reduce Ru^{3+} ions. The reduction reaction was allowed to continue for 2 h under constant and vigorous stirring, after that the final suspension was filtered and washed with deionized water and removed the residue from 50 ml ethylene glycol in the flask. Then, 2.25 mL of 40 mM $PdCl_2$ was added into the flask and heated to 120 ℃under constant stirring for 1 h in an oil bath. After cooling to room temperature, 0.48 mL of 18.9 mM $Bi(NO)_3$ was then added dropwise into the above suspension and the alcohol reduction was continued for 2 h. Finally, the resultant suspension was filtered, washed with deionized water and dried in a vacuum oven at 60 ℃ for about 6 h to obtain 3D RuPdBi/NG catalyst. Meanwhile, the optimal atomic ratio of ruthenium to palladium and bismuth is 2:1:0.1 and to obtain this catalyst, reactions with different atomic ratios of metals to obtain a series of catalysts were synthesized following the same steps as described previously. In addition, 3D Pd/NG and 3D RuPd/NG were produced following the same steps as mentioned above for the purpose of comparison.

2.2. Characterization

The powder X-ray diffraction (XRD) measurements were conducted using Rigaku D/max-3C X-ray diffractometer (Rigaku Corporation, Tok**y**o, Japan) with CuKα as a source of radiation (λ=0.15406 nm) in the 2θ angle range between 10 and 90° at a scan rate of 5°/min with a step size of of 0.02º. The transmission electron microscopy (TEM) was used for the analysis of the morphology and size distribution of the synthesized catalystsand was conducted by JEOL JEM-1010 (200 kV). The electronic states of Ru, Pd and Bi in 3D RuPd/NG (2:1) and 3D RuPdBi/NG (2:1:0.1) samples were investigated by an X-ray photoelectron spectroscopy (XPS; Thermo ESCALAB 250Xi, Thermo Fisher Scientific, Shanghai, China) with an AlKα X-ray source of 1487 eV and the working power was 12.5 kV. In this the chamber pressure was kept below 3×10^{-10} mbar and specific correction was conducted by using a C 1s binding energy of 285 eV. In the catalyst, the exact amounts of Ru, Pd and Bi measured using an IRIS Intrepid Ⅱ XSP inductively coupled plasma atomic emission spectrometer (ICP-AES).

2.3 Electrochemical measurements

All the electrochemical tests were performed by using a CHI660C electrochemical working station (CH Instrument Inc., Bee Cave, Texas). Glassy carbon electrode (12.56 mm2) modified with catalyst was used as the working electrode. A mercury electrode (Hg/HgO/1 M KOH, 0.098V versus SHE) [36] was used as the reference electrode, and a platinum electrode was used as the counter electrode. For the catalytic electrode preparation, 5 mg catalyst was dispersed in a mixture of isopropyl alcohol (910 μL) and 5 wt.% Nafion (90 μL) solution (Hesen, China) under ultrasonic stirring for 30

min. Then 3 μL of catalyst containing dispersion was drop casted on the working electrode surface uniformly. The working electrode was polished with Al_2O_3 powder and rinsed by double-distilled water 10 minutes before using. The working electrode was dried at room temperature for 20 min. Before the electrochemical measurements, the electrolyte (1 M KOH or 1 M KOH +0.5 M $C_2H_6O_2$) was deaerated with pure nitrogen for about 25 min. All the electrochemical measurements were conducted at the room temperature of 25 ℃.

3. RESULTS AND DISCUSSION

The chemical composition of 3D RuPdBi/NG catalyst is obtained by using ICP-AES, which suggests that the actual loading of Ru, Pd and Bi in the final catalyst was 5.7%, 3.37% and 0.83%, respectively. The ratio of atoms in 3D RuPdBi/NG is about 2:1:0.1 which has the best catalytic efficiency which confirms the formation of 3D catalyst. However, the measured content is lower than the amount that was added initially. It may be due to that both ruthenium and palladium were not reduced entirely by $NaBH_4$ and $C_2H_6O_2$. In addition, the content of Bi is so small that it is difficult to obtain a very accurate data.

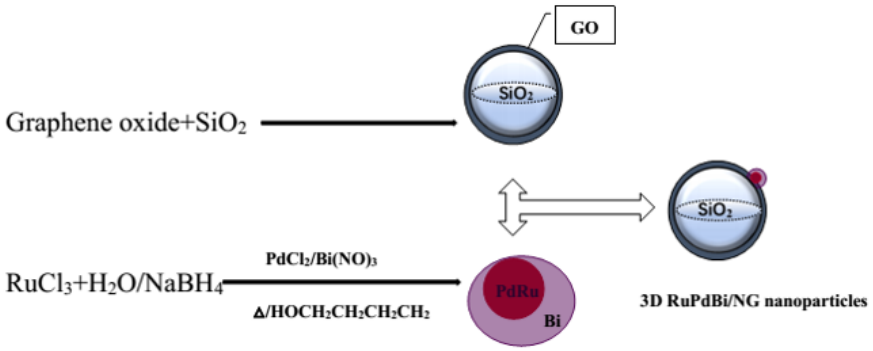

Scheme 1. Synthesis process of RuPdBi/NG nanoparticles

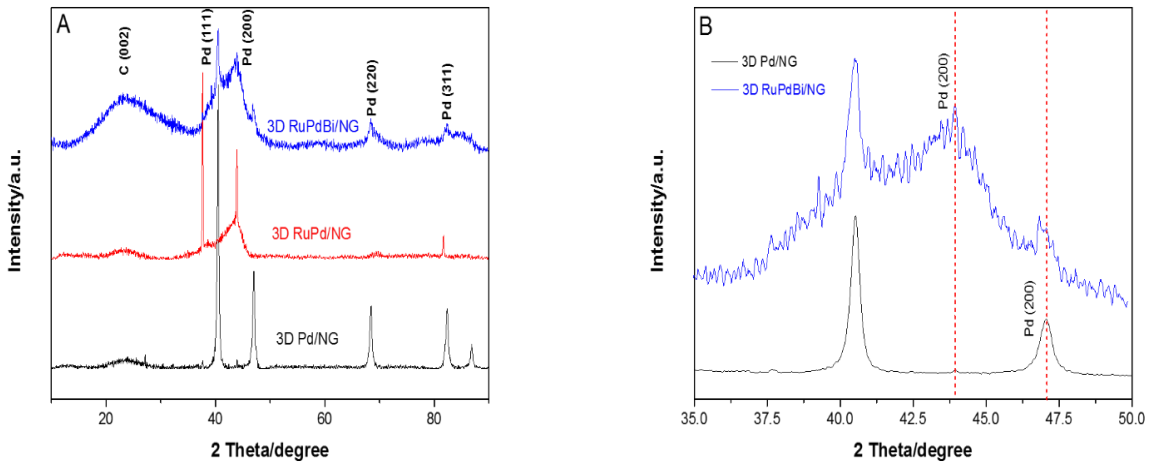

Figure 1. (A) X-ray diffractograms patterns of 3D Pd/NG, 3D RuPd/NG, 3D RuPdBi/NG; (B) X-ray diffractograms patterns of 3D Pd/NG ,3DRuPdBi/NG at 2 Theta 35.0 to 50.0.

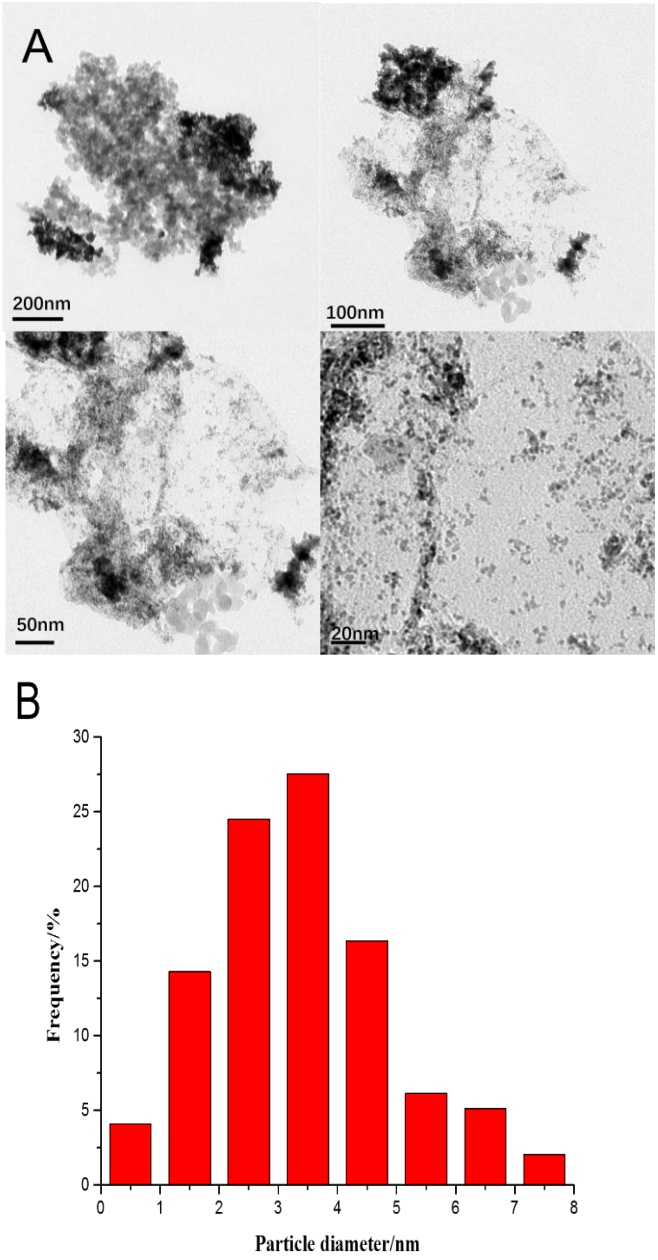

Figure 2. (A)TEM micrographs of 3D RuPdBi/NG; (B) particle size distribution histograms;

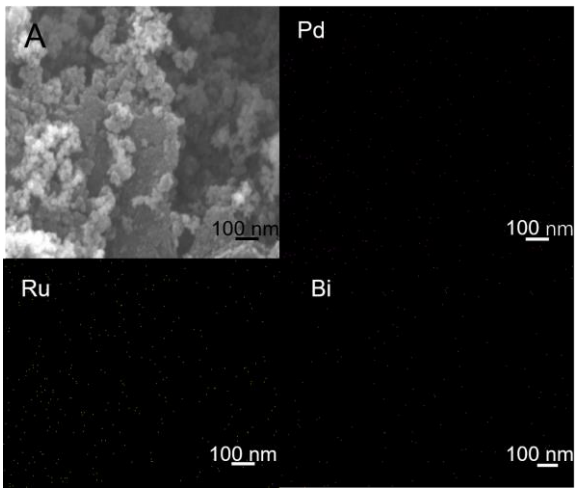

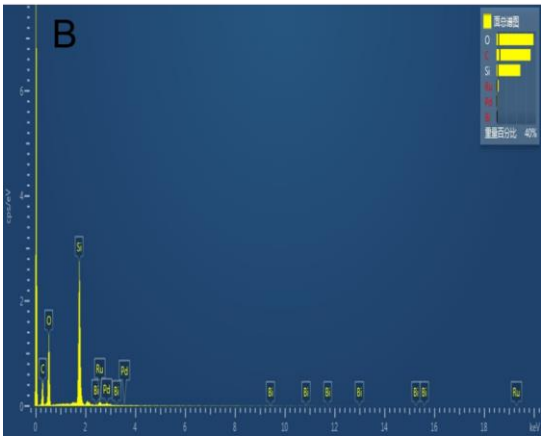

Figure 3. (A) EDX element distribution of Ru, Pd and Bi; (B) Statistics of EDX element distribution.

Fig. 1A shows the XRD patterns of 3D RuPdBi/NG. As can be seen, the peak of about 25.7° indicates (0 0 2) plane of NG hexagonal structure. The 2θ peaks at about 39.8°, 46.1°, 67.6° and 81.2° are corresponding to the (1 1 1), (2 0 0), (2 2 0) and (3 1 1) reflections of palladium's face-centered cubic crystal. Besides, diffraction peaks of Ru or Bi could not be seen neither in the XRD patterns of 3D RuPdBi/NG nor in the 3D RuPdBi/NG. Such a result implies that Ru and Bi exist in the form of amorphous phase or the deposited bismuth is so small that it cannot be observed on the Pd surface using XRD analysis [37]. In addition, the Pd (2 0 0) peak of 3D RuPdBi/NG presents a significant negative shift from the standard Pd peak of (2 0 0). The γ_{met} of Pd, Ru and Bi are at 137 pm, 134 pm and at 160 pm, respectively. The reason behind the shift could be due to the coalescence of Ru lattice with Pd lattice which makes the average γ_{met} shorter as shown in Fig. 1B [38].

Fig. 2A shows the morphology of 3D RuPdBi/NG catalyst using TEM. The nitrogen-doped graphene scaffolds show a three-dimensional network of self-assembled nitrogen-doped graphene spheres. The uniform coating of NG sheets onto SiO_2 templates in the SiO_2@NG network. As observed in Fig. 2A, most of the metal nanoparticles are dispersed in an orderly manner onto NG's surface, with less agglomeration.

The scanning electron Microscopy (SEM) was employed to observe the structure of 3D RuPdBi/NG. The wrinkles and folds that could be observed on the surface of SiO_2 spheres are characteristic of NG sheets. Besides, the NG-wrapped SiO_2 spheres could easily be bridged by NG sheets attributing to their relatively larger lateral sizes, yielding a 3D interconnected hybrid network. The truncated surface of NG in Fig. 3A illustrates this phenomenon. EDX elemental distribution maps in Fig. 3A show that Ru, Pd and Bi particles are uniformly dispersed onto NG surface. The particle size distribution is based on the measurement of 100 non-agglomerated nanoparticles in any selected region of the SEM image; the diameter of major tri-metal nanoparticles is in the range from 2 -5 nm as observed in Fig. 2B. Such a highly uniform dispersion plays an important role to improve the performance of the catalyst. The elemental distribution using EDX is shown in Fig. 3B, which is consistent with the ICP results.

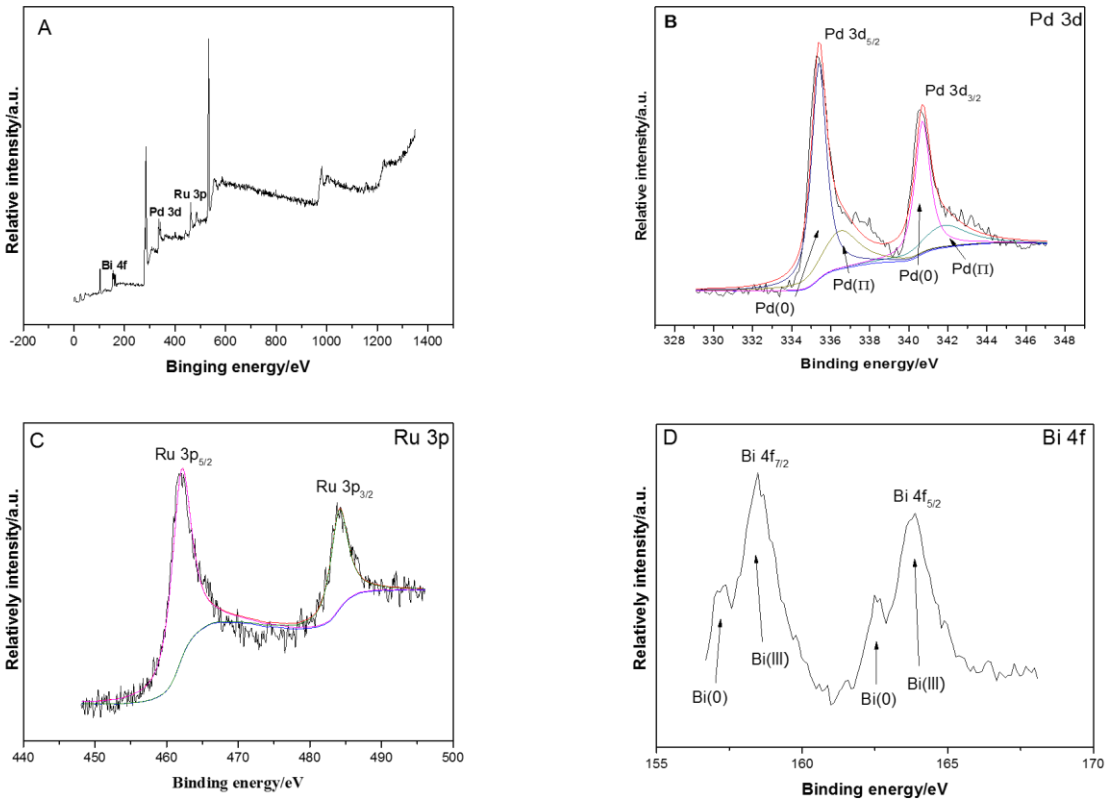

Figure 4. (A) The XPS results of 3D RuPdBi/NG. (B) 3D RuPdBi/NG in Pd 3d; (C) 3D RuPdBi/NG in Ru 3p; (D)RuPdBi/NG in Bi 4f.

X-ray photoelectron spectroscopy (XPS) was used to analyze the metallic states in 3D RuPdBi/NG catalysts. A typical XPS spectra of the as-prepared 3D RuPdBi/NG catalyst is shown in Fig. 4A, which includes Ru, Pd, and Bi peaks. As observed in Fig. 4B, the 3d spectra of Pd split into two asymmetric peaks, which relegated to $3d_{5/2}$ and $3d_{3/2}$. The $3d_{5/2}$ (335.28 and 336.68 eV) has lower binding energies than $3d_{3/2}$ (340.58 and 342.08 eV) about 5.3 eV in each corresponding peak. The weak doublet peak corresponds to Pd (Ⅱ) while the strong doublet peak is attributed to Pd (0) species such as PdO and $Pd(OH)_2$ [39, 40]. In Fig. 4C, the doublet peaks at 461.78 eV (Ru $3p_{5/2}$) and at 483.78 eV (Ru $3p_{3/2}$) belong to pure Ru in the final catalyst [41, 42]. In Fig. 4D, in the Bi 4f region, the peaks of Bi $4f_{7/2}$ and $4f_{5/2}$ at 158.78 and at 163.88 eV are the representation of Bi (Ⅲ). Having the same pattern, the peaks at 157.38 and 163.88 eV belong to Bi (0) [43]. The existence of Bi (0) states clearly indicate that in the process of adsorption and desorption a number of Bi^{3+} ions were reduced, even some were reduced by Pb (0) species. The analysis of XPS shows that Ru and Bi are strongly linked to catalytic Pd and interact with each other, which could affect the catalytic activity of the catalysts.

Fig. 5A shows the cyclic voltammograms (CVs) obtained in 1 M KOH for the 3D RuPdBi/NG catalyst under nitrogen saturated condition. The potential window was chosen from -0.9 V to +0.4 V at a scan rate of 50 mVs^{-1}. Also, the 3D Pd/NG and 3D RuPd/NG were also demonstrated or comparison. As shown in Fig. 5A, a wide peak from -0.9V to -0.6V can be observed in the negative potential

window, which can be attributed to the hydrogen desorption peak, probably due to Bi which is not completely deposited on the surface of Pd [44].

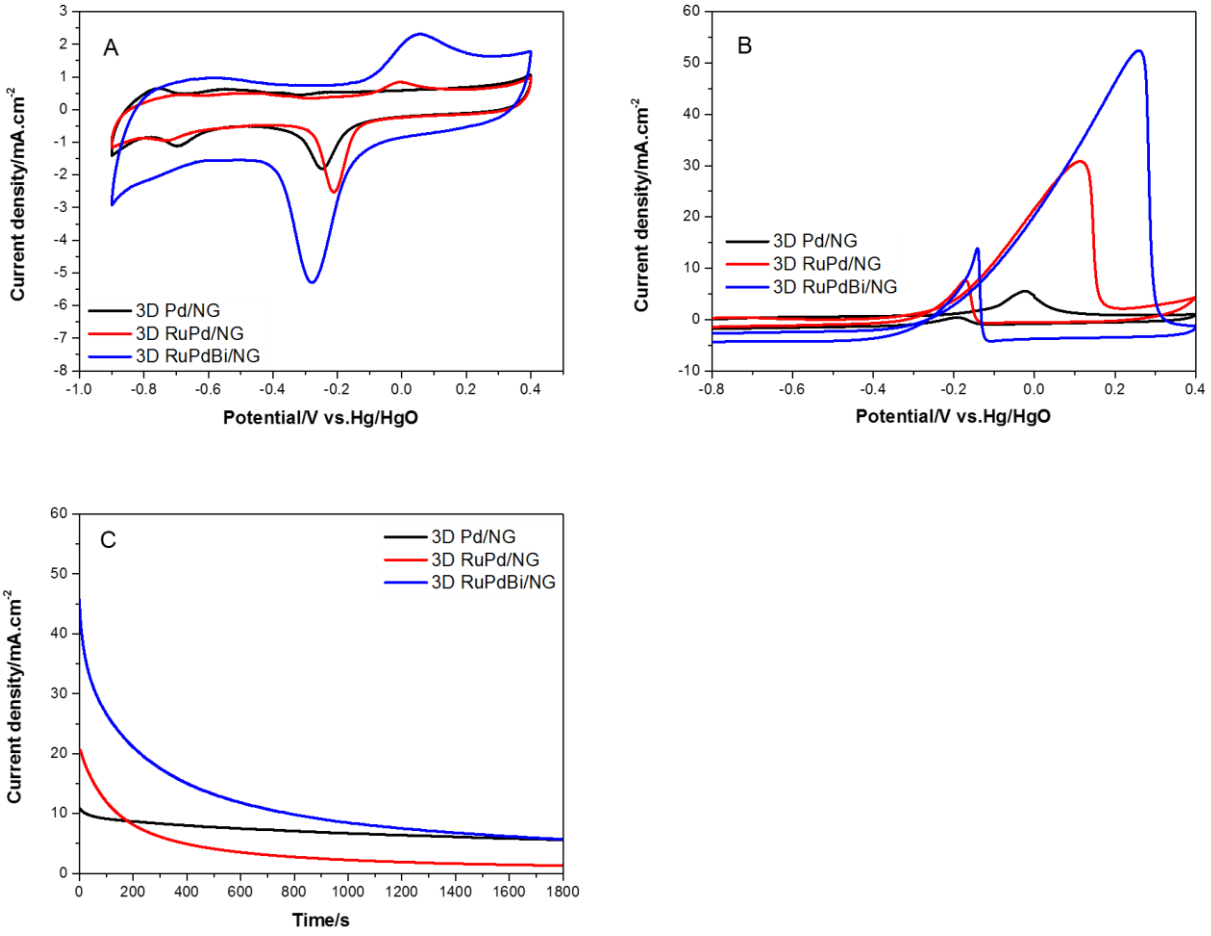

Figure 5. 3D Pd/NG, 3D RuPd/NG and 3D RuPdBi/NG of Cyclic voltammograms test result in (A) 1 M KOH; (B) 1 M KOH +0.5 M $C_2H_6O_2$ at Scan rate 50 mVs-1; (C) Corresponding current time curves carry out at -0.15V.

Table 1. Electrocatalysts for ethylene glycol oxidation

Number	Support material	Loaded material	Amount of loaded material	Catalytic efficiency	Ref.
1	3D nitrogen-doped graphene	Ru, Pd and Bi	Extremely low	Relatively high	This study
2	XC-72R carbon black	Pd, Ir	Normal	Relatively	52

				low	
3	Sulfonated multi-walled carbon nanotubes	PdSn and PdNi	Normal	High	53
4	MexOy promoted XC-72 carbon	Au	Normal	High	54
5	Composite of nanosized carbides and carbon aerogel	Pd	Normal	High	55
6	None	Bimetallic PdPt nanowire networks	High	High	56
7	Phenanthroline modified carbon (PMC)	Pd	Normal	Normal	57
8	XC-72R carbon black	Heterostructured Pd-Ag	Normal	High	58
9	None	NiPt truncated octahedral nanoparticles	High	High	59
10	XC-72R carbon black	Pd,Mo nanocubes	Normal	High	60

In all the catalysts, the characteristic peaks appear in the potential region of -0.2 V to +0.2 V owing to the presence of O_2 evolution [45]. The occurrence of these characteristic peaks could be attributed to the slow conversion from Pd metal to Pd (Ⅱ) oxide. At the potential of about +0.01 V, a prominent peak appears which is due to the surface oxidation of Bi adsorbed on the surface of Pd particles. In addition, during the electrochemical measurements, some of the oxygenated species could be generated and located on the Pd particles' surface which is critical to the electro-oxidation of smaller organic molecules. By means of bifunctional mechanism and ligand effect, the intermediate products adsorbed on the catalyst surface are removed [46, 47]. In the negative potential sweep during CV, an intense reduction peak in the range of -0.20 V to 0.28 V could be observed, which is due to Pd (Ⅱ) oxidation to the element Pd (0) [48]. Especially, the 3D RuPdBi/NG catalyst appears as a single peak which is significantly stronger than other catalysts.

Fig. 5B shows the electrocatalytic activity measurement which was conducted under N_2-saturated condition. CVs were run in 1 M KOH + 0.5 M $C_2H_6O_2$ solution at a scan rate of 50 mV s^{-1}. In the positive scan, the ethylene glycol oxidation current rises gradually with the potential sweep, reaching its maximum oxidation current then starts falling rapidly. The asymmetric peak of 3D RuPdBi/NG catalyst indicates that the diffusion limits the rate of oxidation reaction at a high potential. The CV measurements of RuPdBi reveal the best electrocatalytic activity and the most negative onset potential of ethylene glycol oxidation. The oxidation current peaks of 3D Pd/NG, RuPd/NG, RuPdBi/NG are at 5.55 mA cm^{-2}, 30.8 mA cm^{-2}, and 52.4 mA cm^{-2}, respectively. The 3D RuPdBi/NG (52.4 mA cm^{-2}) catalyst is about 1.5 times of commercial Pd/C (37.0 mA cm^{-2}) catalyst. External bismuth can promote the electrocatalytic oxidation of ethylene glycol in the catalyst by removing the toxic species and exposing the active sites of Pd which leads to the best performance of the 3D RuPdBi catalyst. [49-51]

The long-term activities of these Pd-based catalysts were evaluated in 1 M KOH + 0.5 M $C_2H_6O_2$ at E = -0.15V as shown in Fig. 5C. The current densities of all catalysts descend fast at the beginning stage which demonstrates that the active site of Pd is adsorbed by the toxic species generated in the process of electro-oxidation rapidly and steadily. Besides, the toxic species can hinder further adsorption and oxidation of ethylene glycol. After the initial stage, the current densities decline very slowly and reached a relatively stable period for the relative balance between adsorption of oxygenated and adsorption of toxic species in a redox reaction. The stable current densities of catalysts are as follow: 3D RuPdBi (5.81 mA cm^{-2}) > 3D Pd (5.61 mA cm^{-2}) > 3D RuPd (1.43 mA cm^{-2}). The commercial Pd/C catalyst shows a current density of 1.25 mA cm^{-2}. Which show that 3D RuPdBi/NG catalyst can induce the formation of oxygen species on the catalyst surface, thereby can promote the oxidative removal of the absorbed toxic species from the surface, providing a reaction site for the continuous oxidation of ethylene glycol. Therefore, these catalysts present the best catalytic activity and the results are consistent with the measurements of ethylene glycol oxidation.

A comparison mainly about the ethylene glycol oxidation electrocatalysts' materials has been shown in Table 1. From the comparison, it shows that this kind of 3D electrocatalyst has its application prospect. [52-60]

4. CONCLUSION

In this work, we proposed a new type of 3D RuPdBi/NG catalyst which showed high catalytic activity (52.4 mA cm^{-2}) for ethylene glycol oxidation, which is about 1.5 times higher than commercial Pd/C catalyst. However, the mass of loaded Pd was only 3.37% in this catalyst. As for comparison, the commercial catalyst accounts 20% or more (by mass) of the loaded metals. Whereas, the mass did not exceed 9.9% for the new catalyst. More than a half in the loaded metal was Ru, which is much cheaper and has relatively large storage capacity and moreover, it has better sustainability against toxicity. These results make the newly synthesized catalyst potential to exploit for further commercialization. Especially the synthetic effects of ruthenium and external bismuth induce the formation of oxygen species on the catalytic surface of 3D RuPdBi catalyst to oxidize the toxic species adsorbed on the

surface are responsible for the high electrocatalytic activity of 3D RuPdBi catalyst. Overall, the current research investigation provides a new catalyst structure and a new concept to study the advanced palladium-based catalysts.

ACKNOWLEDGEMENTS
This work was financially supported by the Natural Science Fund for Creative Research Groups of Hubei Province (2014CFA015) of China and the Hubei College Students' Innovation Training Program of China (201410512024, 201510512030).

References

1. M. Winter, R.J Brodd, *Chem. Rev.*, 104 (2004) 4245.
2. A.B.A.A. Nassr, I. Sinev, M.M. Pohl, W. Grunert, M. Bron, *ACS Catal*., 4 (2014) 2449.
3. J.D Cai, Y.Y Huang, Y.L Guo, *Int. J. Hydrogen Energy.*, 39 (2014) 18256.
4. S.M.M. Ehteshami, S.H. Chan, *Electrochim. Acta.*, 93 (2013) 334.
5. S. Song, P. Tsiakaras, Appl. Catal., B., 63 (2006) 187.
6. T. Maiyalagan, K. Scott, *J. Power Sources.*, 195 (2010) 5246.
7. A. Serov, U. Martinez, and P. Atanassov, *Electrochem. Commun.*, 34 (2013) 185.
8. C. Bianchini and P.K. Shen, *Chem. Rev.*, 109 (2009) 4183.
9. A. Zalineeva, A. Serov, M. Padilla, U. Martinez, K. Artyushkova, S. Baranton, C. Coutanceau, and P. Atanassov, *J. Am. Chem. Soc.*, 136 (2014) 3937.
10. U. Martinez, A. Serov, M. Padilla, and P. Atanassov, *ChemSusChem.*, 7 (2014) 2351.
11. W. Liu, A. Herrmann, D. Geiger, L. Borchardt, F. Simon, S. Kaskel, N. Gaponik, and A. Eychm¨uller, *Angew. Chem., Int. Ed*., 51 (2012) 5743.
12. Z. Wena, S. Yangb, Y. Liang, W. He, H. Tong, L. Hao, X. Zhang, and Q. Song, *Electrochim. Acta.*, 56 (2010) 139.
13. E. Antolini, *Energy Environ. Sci.*, 2 (2009) 915.
14. E.E. Switzer, T.S. Olson, A.K. Datye, P.Atanassov, M.R. Hibbs, and C.J. Cornelius, *Electrochim. Acta.*, 54 (2009) 989.
15. W. Du, K.E. Mackenzie, D.F. Milano, N.A. Deskins, D. Su, and X. Teng, *ACS Catal.*, 2 (2012) 287.
16. R.M. Modibedi, T. Masombuka, and M.K. Mathe, *Int. J. Hydrogen Energy.*, 36 (2011) 4664.
17. N. Mackiewicz, G. Surendran, H. Remita, B. Keita, G. Zhang, L. Nadjo, A. Hag`ege, E. Doris, and C. Mioskowski, *J. Am. Chem. Soc.*, 130 (2008) 8110.
18. M. Zhang, J Xie, Q Sun, Z. Yan, M. Chen, J. Jing, and A.M. Hossain, *Electrochim. Acta.*, 111 (2013) 855.
19. Z. Zhang, L. Xin, K. Sun, and W. Li, *Int. J. Hydrogen Energy.*, 36 (2011) 12686.
20. C. Xu, L. Cheng, P. Shen, Y. Liu, *Electrochem. Commun.*, 9 (2007) 997.
21. Y. Wang, F.F. Shi, Y.Y. Yang, W.B. Cai, *J. Power Sources.*, 243 (2013) 369.
22. L. Zhang, Y. Tang, J. Bao, T. Lu, C. Li, *J. Power Sources.*, 162 (2006) 177.
23. Liu, X. Cai, J. Wang, J. Liu, A. Riese, Z. Chen, X. Sun, S.D. Wang, *Int. J. Hydrogen Energy.*, 41 (2016) 13476.
24. T. Li, Y. Huang, K. Ding, P. Wu, S.C. Abbas, M.A. Ghausi, T. Zhang, Y. Wang, *Electrochim. Acta.*, 191 (2016) 940.
25. L. Castanheira, L. Dubau, M. Mermoux, G. Berthom´e, N. Caqu´e, E. Rossinot, M. Chatenet, and F. Maillard, *ACS Catal.*, 4 (2014) 2258.
26. L. Dubau, F. Maillard, M. Chatenet, L. Guetaz, J. Andre, and E. Rossinot, *J. Electrochem. Soc.*, 157 (2010) B1887.
27. W.S. Hummers and R.E. Offeman, *J. Am. Chem. Soc.*, 80 (1958) 1339.

28. P.J. Ferreira, G.J. la O', Y. Shao-Horn, D. Morgan, R. Makharia, S. Kocha, and H.A. Gasteiger, *J. Electrochem. Soc.*, 152 (2005) A2256.
29. Z. Zhao, L. Dubau, and F. Maillard, *J. Power Sources.*, 217 (2012) 449.
30. E. Guilminot, A. Corcella, F. Charlot, F. Maillard, and M. Chatenet, *J. Electrochem. Soc.*, 154 (2007) B96.
31. A. Serov, N.I. Andersen, S.A. Kabir, A. Roy, T. Asset, M. Chatenet, F. Maillard, P. Atanassov, *J. Electrochem. Soc.*, 162 (2015) 1305.
32. W.S. Hummers, R.E. Offeman, *J. Am. Chem. Soc.*, 80 (1958) 1339.
33. T. Chen, B. Zeng, J. Liu, J. Dong, X. Liu, Z. Wu, X. Yang, Z. Li, J. Phy.: *Conference Series.*, (2009) 012051.
34. S. Li, H. Yang, R. Ren, J. Ma, J. Jin, J. Ma, *J. Power Sources.*, 294 (2015) 360.
35. P. Wu, H. Wang, Y. Tang, Y. Zhou, T. Lu, *ACS Appl. Mater. Interfaces.*, 6 (2014) 3546.
36. R. N. Singh, A. Singh, Anindita, *Int. J. Hydrogen Energy.*, 34 (2009) 2052.
37. Y. Huang, S. Zheng, X. Lin, L. Su, Y. Guo, *Electrochim. Acta.*, 63 (2012) 346.
38. A. Tripković, S.L. Gojković, K.D. Popović, J. Lović, A. Kowal, *Electrochim. Acta.*, 53 (2007) 887.
39. Y. Suo, I. Hsing, *J. Power Sources.*, 196 (2011) 7945.
40. I.G. Casella, M. Contursi, *J. Electroanal. Chem.*, 588 (2006) 147.
41. R. Freitas, L. Marchesi, R. Oliveira, F. Mattos-Costa, E. Pereira, L. Bulhoes, M. Santos, *J. Power Sources.*, 171 (2007) 373.
42. D.R. Rolison, P.L. Hagans, K.E. Swider, J.W. Long, *Langmuir.*, 15 (1999) 774.
43. M. Simões, S. Baranton, C. Coutanceau, *Electrochim. Acta.*, 56 (2010) 580.
44. F.J. Rodríguez-Nieto, T.Y. Morante-Catacora, C.R. Cabrera, *J. Electroanal. Chem.*, 571 (2004) 15.
45. R. Awasthi, R. Singh, *Carbon.*, 51 (2013) 282.
46. M. Li, D.A. Cullen, K. Sasaki, N.S. Marinkovic, K. More, R.R. Adzic, *J. Am. Chem. Soc.*, 135 (2012) 132.
47. M. Chatterjee, A. Chatterjee, S. Ghosh, I. Basumallick, *Electrochim. Acta.*, 54 (2009) 7299.
48. B.F. Machado, P. Serp, *Electrochem. Commun.*, 12 (2010) 1796.
49. Lang F, Liu J, Wang H, *Nano.*, 1750058.
50. J. Luo, P.N. Njoki, Y. Lin, D. Mott, L. Wang, C.J. Zhong, *Langmuir.*, 22 (2006) 2892.
51. A. Tripković, S.L. Gojković, K.D. Popović, J. Lović, A. Kowal, *Electrochim. Acta.*, 53 (2007) 887.
52. J. Chen, G. Wang, X. Wang, J. Tian, S. Zhu, R. Wang, *J. Nanosci. Nanotechnol.*, 13 (2013) 7008.
53. T. Ramulifho, K.I. Ozoemena, R.M. Modibedi, C.J. Jafta, M.K. Mathe, *J. Electroanal. Chem.*, 692 (2013) 26.
54. S. Yongprapat, A. Therdthianwong, S. Therdthianwong, *J. Electroanal. Chem.*, 697 (2013) 46.
55. X. Zhang, Z. Tian, P.K. Shen, *Electrochem. Commun.*, 28 (2013) 9.
56. W. Hong, C. Shang, J. Wang, E. Wang, *Energy Environ. Sci.*, 8 (2015) 2910.
57. Y. Yang, W. Wang, Y. Liu, F. Wang, D. Chai, Z. Lei, *Electrochim. Acta.*, 154 (2015) 1.
58. Y. Yang, W. Wang, Y. Liu, F. Wang, Z. Zhang, Z. Lei, *Int. J. Hydrogen Energy.*, 40 (2015) 2225.
59. T. Xia, J. Liu, S. Wang, C. Wang, Y. Sun, L. Gu, R. Wang, *ACS Appl. Mater. Interfaces.*, 8 (2016) 10841.
60. O. Ambriz-Peláez, L. Álvarez-Contreras, M. Guerra-Balcázar, J. Ledesma-García, L.G. Arriaga, N. Arjona, *ChemElectroChem.*, 4 (2017) 728.